Hot-carrier multijunction solar cells: sensitivity and resilience to nonidealities

Maxime Giteau[a,b,*] **Samy Almosni**[c] **Jean-François Guillemoles**[a,d] **and Daniel Suchet**[a,e,*]

[a]The University of Tokyo, NextPV, CNRS, Tokyo, Japan
[b]CNRS, Centre for Nanoscience and Nanotechnology, Palaiseau, France
[c]Saule Technologies, Wroclaw Technology Park, Wroclaw, Poland
[d]CNRS, Institut Photovoltaïque d'Île-de-France (IPVF), UMR 9006, Palaiseau, France
[e]École Polytechnique, Institut Photovoltaïque d'Île-de-France (IPVF), Palaiseau, France

Abstract. The resilience against non-idealities of hot-carrier multijunction solar cells (HCMJSCs) is assessed and compared with two references, namely a multijunction solar cell (MJSC) and a hot carrier solar cell (HCSC). We investigate the impact on the efficiency of three deviations from the ideal case: nonoptimal design, internal limitations, and nonstandard operation conditions. We show that the HCMJSC maintains a high efficiency even when materials with nonoptimal bandgaps are considered, broadening the range of candidate materials for its implementation. We also show that the requirement for hot carriers' thermalization is much less stringent than with the standard HCSC architecture, allowing to surpass the best MJSC efficiency with currently achievable thermalization coefficients. Finally, we estimate the influence of nonstandard illumination by varying the AM spectrum and estimate numerically the yearly averaged efficiency of devices installed in two different locations. Preliminary results on temperature dependence are also presented. [DOI: 10.1117/1.JPE.12.032208]

Keywords: hot carrier; tandem; solar cell; high efficiency; resilience.

Paper 22015SS received Mar. 1, 2022; accepted for publication Apr. 26, 2022; published online Jun. 1, 2022.

1 Introduction

Increasing the power conversion efficiency (PCE) of solar cells is an unending challenge that has stimulated intense research activity. Standard single-junction systems are ultimately limited to 30% efficiency (the celebrated Shockley–Queisser limit[1,2]) by the trade-off between light absorption and carriers' thermalization. As laboratory prototypes approach this theoretical limit, alternative strategies are scrutinized to circumvent these constraints and reach higher efficiencies.

Several advanced concepts[3] have been shown theoretically to allow conversions at yields close to the thermodynamic limit at 86%. Among them, hot carrier solar cells (HCSCs) offer a promising route, by harvesting the energy of photogenerated carriers before they dissipate their excess of kinetic energy.[4–6] However, most of the advanced proposals have not in practice allowed the Shockley–Queisser limit to be exceeded yet. Furthermore, even systems with nominal efficiency above this value, such as multijunction solar cells (MJSCs), do not perform as well as expected when operated in real conditions.[7]

A possible key to understand the difficulties met by advanced concepts resides in their vulnerability to nonidealities. Indeed, it appears that while ideal systems are expected to reach ultrahigh efficiencies, the introduction of even a limited amount of imperfections can reduce the yield down to (or even below) the Shockley–Queisser limit. Such deviations from ideal conditions can occur from nonoptimal design (material bandgap, layer thickness, etc.), from internal imperfections of the device (nonradiative recombination, limited absorptivity, and finite thermalization coefficient[8]), or from the operating conditions (ambient temperature[9,10] and illumination

*Address all correspondence to Maxime Giteau, maxime.giteau.pro@gmail.com; Daniel Suchet, daniel.suchet@polytechnique.org

spectrum[11]). As a case in point, Shpaisman et al.[12] have shown in a practical case that, while the combination of multiple exciton generation and up-conversion promises a PCE of 49% in the ideal case, it is actually limited to 38% even with optimistic (but nonideal) efficiencies for the multiple-exciton generation (MEG) and up-conversion (UC) processes.

It thus appears that conversion strategies should be considered not only from the perspective of their ideal efficiency but also considering their resilience to nonidealities. For instance, the introduction of an energy ratchet in intermediate band solar cells offers only a minute increase in the system's efficiency in ideal conditions,[13] but most importantly prevents the efficiency from collapsing when internal nonidealities are considered.[14,15] As another example, it appears that HCSCs are less sensitive to spectral variations than MJSCs with similar efficiencies,[16,17] allowing them to maintain high efficiency even as the solar radiation deviates from the standard AM1.5D spectrum under which nominal performances are estimated. Averaged over the year, this resilience allows HCSCs to feature a better performance ratio than their MJ counterparts,[17] resulting in a larger (potential) energy production.

In this work, we estimate and compare the resilience of the HCSC and MJSC to a novel architecture called hot-carrier MJSC (HCMJSC). This device consists of a thin HC top junction series connected to a thick cold bottom junction.[18] We first detail the model used to evaluate the efficiency of the three architectures, highlighting the underlying optical model. We then show that HCMJSC maintains high efficiency even with nonoptimal materials. Finally, we consider the sensitivity of these technologies to operation conditions. We discuss the performance ratio of devices installed at specific locations frequently considered in the literature (Solar Village in Saudi Arabia and Golden, Colorado, United States) and evaluate their fundamental temperature coefficients.

2 Model

The evaluation of the devices' efficiency is based on a detailed-balance model approach.[1,19,20] Compared with the original model developed by Shockley and Queisser,[1] our model combines several additional features: it accounts for multiple junctions, hot-carrier effects, and implements a Beer–Lambert absorption model. This model is the same as the one implement in Ref. 18 and is described here in more detail.

2.1 *General Assumptions*

We assume, as in the original model, that all recombinations are radiative. In steady-state operation, the current $J_{\mathrm{ext},i}$ extracted from each junction must verify

$$J_{\mathrm{ext},i} = J_{\mathrm{abs},i} - J_{\mathrm{rad},i}, \tag{1}$$

where $J_{\mathrm{abs},i}$ is the photogenerated current density in layer i and $J_{\mathrm{rad},i}$ is the recombined current density (We do not consider luminescent coupling between the junctions). The photogenerated current density is estimated as

$$J_{\mathrm{abs},i} = q \int \mathrm{d}E A_i(E) \Phi_i(E), \tag{2}$$

where $A_i(E)$ is the absorptivity of layer i, $\Phi_i(E)$ is the incident photon flux, and q is the electron charge. In MJ systems, $\Phi_1(E) = \Phi_{\mathrm{sun}}(E)$ and $\Phi_2(E) = (1 - A_1(E))\Phi_{\mathrm{sun}}(E)$, where $\Phi_{sun}(E)$ is the photon flux received from the sun (this can directly be generalized to three or more junctions).

The recombination current density (assumed to be fully radiative for simplicity) is derived from the generalized Planck law[21]

$$J_{\mathrm{rad},i} = \frac{2\pi q}{h^3 c^2} \int \mathrm{d}E A_i(E) \frac{E^2}{\exp\left(\frac{E-\Delta\mu_i}{k_B T_i}\right) - 1}, \tag{3}$$

where $\Delta\mu_i$ is the quasi-Fermi level splitting (QFLS) between electrons and holes and T_i is the carrier temperature in layer i, h is the Planck constant, k_B is the Boltzmann constant, and c is the speed of light in vacuum. This expression assumes light is emitted uniformly in the half space above the cell (a mirror prevents emission from the back of the device).

The output power from each junction is

$$P_i = V_i \times J_{\mathrm{ext},i}, \tag{4}$$

where V_i is the voltage. In absence of HC effects, the carrier temperature is the lattice temperature, and the voltage is simply given by $qV_i = \Delta\mu_i$.

2.2 *Absorption*

A specificity of our approach is the model used for optical absorption. Unlike many detailed balance studies which assume a step-like absorptivity $A_i(E) = \theta(E - E_{g,i})$ (i.e., full absorption of all photons above the bandgap), we describe absorption with a Beer–Lambert (assuming no front-surface reflection) model to account realistically for the thickness-dependent absorptivity of each layer

$$A_i(E) = 1 - \exp(-\alpha_i(E)d_i), \tag{5}$$

where d_i is the optical thickness of the layer and $\alpha_i(E)$ is the material's absorption coefficient. To describe absorption for continuous values of bandgaps $E_{g,i}$, we consider the absorption coefficients of InP ($E_g = 1.34$ eV) and GaInAs ($E_g = 0.74$ eV), and perform a linear extrapolation to obtain absorption coefficients for bandgaps between 0.6 and 1.8 eV.[18]

Furthermore, we take into account the impact of the photogenerated band filling on the absorption coefficient[22]

$$\alpha_i(E) = \alpha_{i,0}(E)\tanh\left(\frac{E - \Delta\mu_i}{4k_B T_i}\right), \tag{6}$$

where we assumed identical effective masses for electrons and holes for simplicity.

This careful estimation of the absorptivity [Eqs. (5) and (6)] is important for MJ devices, where an overestimation of the top cell absorption leads to an incorrect current matching with the bottom cell.[23] It is even more crucial for HCSCs, since HC effects are much stronger in ultrathin absorbers[24,25] which are prone to band filling and offer a limited optical thickness.

2.3 *Multiple Junctions*

To model tandem junctions, the detailed balance equations are solved for each subjunction separately. The flux that reaches the second junction is the incident photon flux minus the fraction absorbed in the first junction, neglecting additional parasitic absorption.

For four-terminal devices, the maximum output power is simply the sum of the optimal powers produced by each junction $P^{\max} = \sum(P_i^{\max})$. For two-terminal devices, an additional current-match constraint must be considered. For simplicity, the current of the device is fixed to that of the current-limiting cell, and the overall optimum output power is found by determining the voltage for that current in the nonlimiting cell

$$P^{\max} = J_{\mathrm{ext},l}^{\max} \times (V_l^{\max} + V_{\mathrm{nl}}(J_{\mathrm{ext},l}^{\max})), \tag{7}$$

where l and nl refer to the current-limited cell and to the not current-limited cell, respectively. This approximation allows a straightforward generalization to any number of junctions.

Finally, the efficiency is given as $\eta = P^{\max}/P_{\mathrm{inc}}$, where $P_{\mathrm{inc}} = \int \mathrm{d}E E\Phi_{\mathrm{sun}}(E)$ is the power flux incident from the sun.

2.4 *Hot-Carrier Junction*

The detailed balance for energy and particles in a hot-carrier junction requires, in addition to current balance [Eq. (1)], a balance for the power flux[4]

$$P_{\mathrm{ext},i} = P_{\mathrm{abs},i} - P_{\mathrm{rad},i} - P_{\mathrm{th},i}, \tag{8}$$

where $P_{\mathrm{ext},i}$ is the power flux extracted from the cell, $P_{\mathrm{abs},i}$ is the absorbed power flux, $P_{\mathrm{rad},i}$ is the radiated power flux, and $P_{\mathrm{th},i}$ is the thermalized power flux. The first two are obtained in the same way as their respective currents [Eqs. (2) and (3)]:

$$P_{\mathrm{abs},i} = \int \mathrm{d}E A_i(E) E \times \Phi_i(E), \tag{9}$$

$$P_{\mathrm{rad},i} = \frac{2\pi}{h^3 c^2} \int \mathrm{d}E A_i(E) \frac{E^3}{\exp\left(\frac{E-\Delta\mu_i}{k_B T_i}\right) - 1}. \tag{10}$$

The voltage is given (assuming isentropic extraction) as[4,20]

$$qV_i = \frac{T_L}{T_i}\Delta\mu_i + \left[1 - \frac{T_L}{T_i}\right]\Delta E_{\mathrm{ext},i}, \tag{11}$$

where T_L is the lattice temperature and $\Delta E_{\mathrm{ext},i}$ is the difference between the extraction energy for electrons and holes (note that we recover the conventional expression $qV_i = \Delta\mu_i$ when $T_i = T_L$). $\Delta E_{\mathrm{ext},i}$ relates the extracted power and current through

$$P_{\mathrm{ext},i} = \Delta E_{\mathrm{ext},i} J_{\mathrm{ext},i}. \tag{12}$$

It is important to note that the extracted power is different from the output power P_i since some power is lost during carrier extraction. All parameters (including the extraction energy) can be derived from two parameters, e.g., the QFLS and the carrier temperature. The maximum power $P_{\mathrm{max},i}$ can be found by optimizing these two parameters. If the extraction energy is fixed, then the parameter space becomes further constrained, potentially reducing the power output.

In an ideal hot carrier solar cell, the cooling of photogenerated carriers is completely inhibited ($P_{\mathrm{th},i} = 0$), allowing the system to reach efficiencies close to the thermodynamic limit.[4] In real systems however, interactions with the lattice cannot be neglected, leading to some power being lost by thermalization. From empirical and theoretical findings,[25] we quantify the thickness-dependent thermalized power through a volume thermalization coefficient q_v (in $\mathrm{W.cm^{-3}.K^{-1}}$)

$$P_{\mathrm{th},i} = q_v d(T_i - T_L). \tag{13}$$

This equation, along with Eq. (5), highlights the trade-off faced by hot-carrier devices, which need to be optically thick while at the same time physically thin.[25] This naturally leads to considering light trapping for these devices.[20,24] We showed previously that within this detailed balance framework, increased light trapping is equivalent to a reduction in the volume thermalization coefficient, leading to the definition of an effective thermalization coefficient.[18,20] Therefore, here we do not introduce light trapping, but keep the volume thermalization coefficient as a free parameter that accounts for both.

2.5 *Simulation Parameters*

We consider as a reference for the incident solar spectrum the ASTM G-173-03 AM1.5D spectrum, which is the standard for evaluating the performance of solar cells under concentration. Its intensity is 90.0 $\mathrm{mW.cm^{-2}}$ for a direct one-sun illumination. We consider a concentration of 1000 suns, which is typical of currently deployed high-concentration PV systems. By default, the temperature of the lattice is 300 K.

Several parameters can be optimized in each type of device. The bandgaps E_g and optical thicknesses d can be adjusted for both junctions. We always consider optically thick (2 μm) HCSCs to ensure good light absorption. The bottom junction for HCMJSCs and MJSCs is also considered thick (2 μm) for the same reason. For the top cell, it is always thick for MJSCs (2 μm), while its thickness is adjusted to ensure current matching in HCMJSCs. In hot-carrier devices, there are two additional parameters: the thermalization coefficient q_V and the extraction energy ΔE_{ext}.

3 Resilience to Nonoptimal Design

Using the model introduced in the previous section, we first estimate the maximal efficiency of the structures under scrutiny and consider the impact of deviations from the optimal design.

We present in Fig. 1 the maximum efficiency of (a) an HCMJSC and (b) an HCSC as a function of the bandgap of the top cell and the thermalization coefficient. For the HCMJSC, the bandgap of the bottom cell is fixed to 0.93 eV, which we previously showed to be close to optimal for all configurations.[18] An ideal HCSC under 1000 sun AM1.5D illumination, may reach an efficiency of 78.9 % when the bandgap is very small (below 480 meV[4]). In this ideal case, the thermalization coefficient is assumed to be zero. However, as soon as a finite thermalization rate is taken into account, the efficiency of the HCSC decreases significantly[26,27] [see Fig. 1(b)].

The optimal efficiency of the HCMJSC is smaller since the photons absorbed in the bottom junction always lose their extra energy through thermalization. However, it is less impacted by partial thermalization than HCSC and therefore can achieve higher efficiencies than HCSCs as soon as we move away from ideal conditions [see Fig. 1(a)]. Qualitatively, the HCMJSC architecture provides an additional degree of freedom as compared with the standard HCSC design by adjusting the thickness of the top absorber. A mediocre thermalization coefficient can be compensated by thinning the top absorber, which allows for maintaining a significant hot carrier effect. In an HCSC, this strategy would lead to a net decrease in the devices' absorptivity, which cannot be compensated. In an HCMJSC, the bottom cell can convert part of the absorbed photons, improving the trade-off.

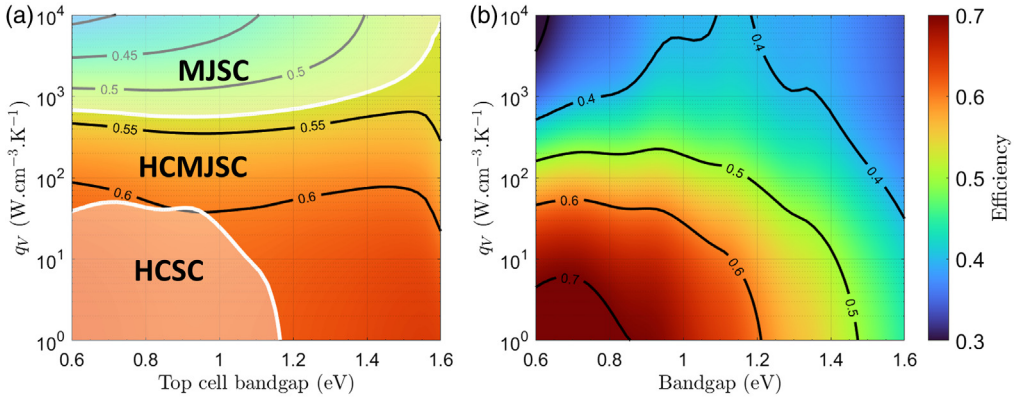

Fig. 1 Efficiency of a HC device as a function of the bandgap of the HC cell and the thermalization coefficient q_V, under 1000 sun illumination (AM1.5D spectrum). The absorption coefficients are extrapolated from InP and InGaAs lattice-matched to InP. For the HCMJSC device (a), the bottom cell has a bandgap of 0.93 eV (close to optimal for all configurations) and an optical thickness of 2 μm. The optical thickness of the top cell is adjusted to ensure current matching for each bandgap. The bottom left shaded region shows material parameters for which a standard HCSC outperforms the HCMJSC. The top shaded region shows material parameters for which the HCMJSC is not as good as the optimal MJSC (defined as $E_{g,\text{top}} = 1.59$ eV and $E_{g,\text{bot}} = 0.93$ eV, corresponding to 53.15% efficiency). Note that, if an MJSC and an HCMJSC were made with the same subcells, the HCMJSC would always outperform the MJSC owing to the efficiency boost of hot carriers. For the HCSC device (b), the optical thickness of the cell is considered to be 2 μm.

As a result, for a simple HCSC to surpass an HCMJSC designed with similar materials, the thermalization factor q_V needs to be below 50 W.cm^{-3}.K^{-1} if the material has a well-suited bandgap. For comparison, the thermalization coefficient in GaAs was measured to be $q_V \approx 2.10^6$ W.cm^3.K^{-1}. Although many groups have measured much slower thermalization in other materials,[28–32] a significant gap still needs to be bridged to enable high-efficiency HCSCs. As such, the HCMJSC architecture currently appears much more promising than single-junction HCSCs.

For a tandem MJSC operating under standard conditions at 1000 sun concentration, the optimal design corresponds to a thick (2 μm) top cell with a 1.59 eV bandgap and an equally thick bottom cell with a 0.93 eV bandgap, allowing an efficiency of 53.15%. Note that this bandgap combination cannot be achieved with a homoepitaxial combination of III–V materials.[33] Even with a 4-terminal (4T) design, which reduces the constrain on current matching at the expense of a more complicated implementation, the efficiency remains quite sensitive to the bandgap of the top junction [Fig. 2(b)].

By contrast, the HCMJSC, with a thermalization coefficient $q_v = 10^3$ W.cm^{-3}.K^{-1}, maintains high efficiency over a much broader range of materials, even with a two-terminals design where current matching is required [Fig. 2(a)]. (While optimistic, this value of thermalization coefficient is not far from what is currently achievable, as argued in Ref. 18.) In particular, an HCMJSC is much less sensitive to the bandgap of the top junction than its MJSC counterpart. Here again, the HCMJSC's advantage comes from the extra degree of freedom in the top absorber thickness. In an HCMJSC, a low-bandgap top junction means a thinner junction (to ensure current matching), which improves the HC effect.

For the optimal design ($E_{g,\mathrm{top}} = 1.59$ eV and $E_{g,\mathrm{bottom}} = 0.93$ eV), the HCMJSC slightly surpasses the MJSC efficiency (54.25%) owing to the hot carrier effect. But most importantly, this novel design is still above 52% efficiency when considering a set of lattice-matched materials such as InP ($E_{g,\mathrm{top}} = 1.34$ eV) on GaAsInP ($E_{g,\mathrm{bottom}} = 0.93$ eV). By contrast, the efficiency of a 4T MJSC falls below 50% with this configuration. The HCMJSC can also be operated efficiently in the double homo-junction configuration ($E_{g,\mathrm{top}} = E_{g,\mathrm{bottom}}$), a configuration which offers very limited benefits relative to the single-junction solar cell for a MJSC.

We summarize our results in Fig. 1(a). As compared with HCMJSCs, single-junction HCSCs are beneficial only for very low thermalization coefficient and small bandgaps (bottom left corner). Compared with an MJSC made with a similar materials, the HC effect in the HCMJSC provides an advantage in terms of efficiency. This allows HCMJSC to display efficiencies better than the best MJSC (top left corner) as soon as the thermalization reaches values $<10^3$ W.cm^{-3}.K^{-1}.

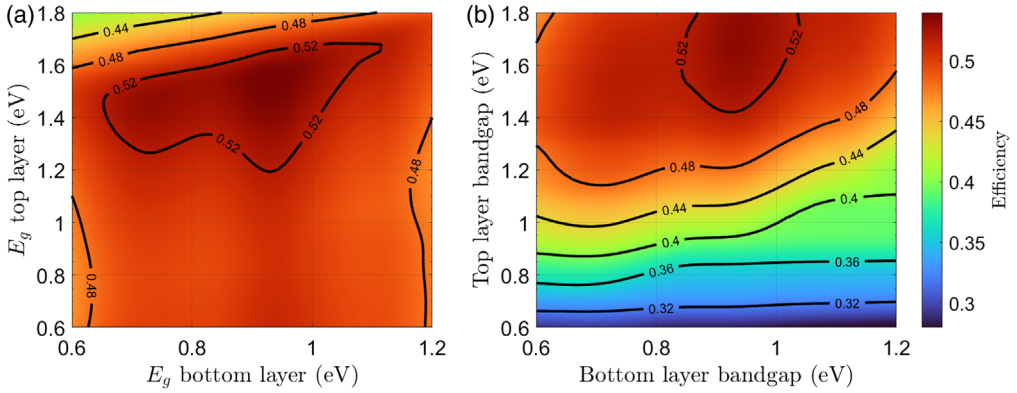

Fig. 2 Efficiency of MJ devices as a function of the bandgap of the top and bottom junctions, under 1000 sun illumination (AM1.5D spectrum). The absorption coefficients are extrapolated from InP and InGaAs lattice-matched to InP. The thickness of the bottom cell is 2 μm. (a) HCMJSC considering a thermalization coefficient $q_V = 10^3$ W.cm^{-3}.K^{-1}. The thickness of the top junction is adjusted for each configuration to ensure current matching (with a maximum of 2 μm). (b) Four-terminal connected MJSC. The thickness of the top junction is always considered to be 2 μm.

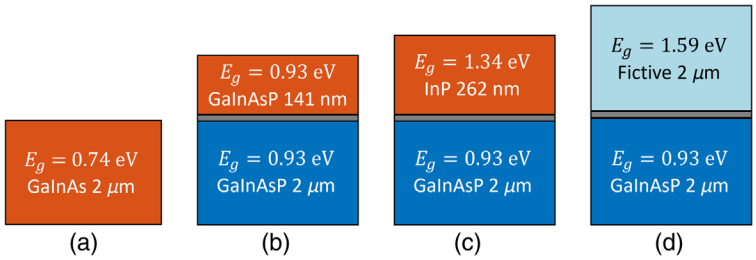

Fig. 3 Devices considered for the influence of nonideal operation conditions. (a) A HCSC with a bandgap $E_g = 0.74$ eV corresponding to GaInAs. (b) A double homojunction HCMJSC with $E_{g,\mathrm{bot}} = E_{g,\mathrm{top}} = 0.93$ eV. (c) A HCMJSC with the same bottom cell but an InP top cell ($E_{g,\mathrm{top}} = 1.34$ eV). (d) The ideal (fictive) MJSC with $E_{g,\mathrm{top}} = 1.59$ eV and $E_{g,\mathrm{bot}} = 0.93$ eV.

4 Resilience to Nonstandard Operation Conditions

We now turn to the evaluation of the resilience of the three technologies against operation conditions, namely spectral variations and lattice temperature variations. To allow a straightforward comparison between the different architectures under scrutiny, we consider four devices with the same efficiency as the ideal MJSC under 1000 sun AM1.5D illumination (53.15%). They are presented in Fig. 3: we consider an HCSC, two HCMJSCs, one in double-homojunction configuration with a narrow top cell bandgap and the other with a wider top cell bandgap, and the ideal MJSC. The thermalization coefficient is adjusted in all hot-carrier devices so their efficiency matches that of the MJSC. All devices are considered in 2T configuration. The extraction energy is fixed along with the other parameters so as to analyze the sensitivity of the devices when operated away from the conditions for which they have been optimized. We verified that the results obtained for the HCSC do not depend significantly on its bandgap.

4.1 *Nonstandard Illumination*

As a standard, nominal cells efficiencies are estimated under a reference illumination (ASTM G-173-03 spectrum) at a reference temperature (300 K). However, real operation conditions will differ from this reference, possibly leading to a degradation of the efficiency. In particular, as the Sun follows its course, solar radiation will have to travel through larger atmospheric depth, which modifies not only the illumination intensity but also its spectral distribution. To estimate the sensitivity of the different structures to spectral variations, we thus focus on the impact of the air mass (AM).

Starting from the atmospheric parameters of the ASTM G-173-03 standard, we computed incident spectra as a function of the air mass using the SMARTS2 software.[34] For each structure, we calculated the efficiency and output power as a function of the air mass (Fig. 4). By design,

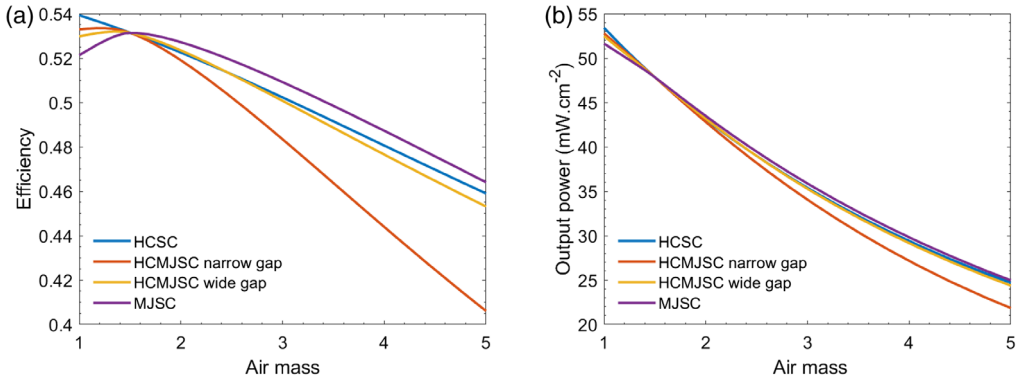

Fig. 4 (a) Efficiency and (b) output power of the four different devices presented in Fig. 3 as a function of the air mass.

all efficiencies are equal at AM 1.5. However, the different technologies have different sensitivity to spectral variations [Fig. 4(a)].

For the MJSC, the efficiency is maximal at AM 1.5, and any variation in the air mass degrades the efficiency. The cell was indeed designed to be current matched for AM1.5D spectrum, and any departure from that point thus leads to current mismatch resulting in a degraded efficiency.

For the HCSC, the efficiency decreases as the AM increases. Qualitatively, as the atmospheric absorption coefficient is larger at shorter wavelength, a longer optical path reduces the population of high-energy photons more than that of low-energy photons. As blue photons contribute most to the hot carrier effect, this spectral shift is detrimental to HCSC. For similar reasons, decreasing the AM actually increases the device's efficiency.

HCMJSCs combine both effects. For AM below 1.5, the two effects compensate as the current mismatch is offset by the increased hot-carrier effect. For AM above 1.5, the two effects cumulate and the efficiency decreases faster than that of a simple HCSC or MJSC. This sensitivity is more limited for HCMJSCs with large top bandgaps, where the hot carriers' contribution is more limited.

The degradation of PCE with Air Mass should however be considered in regards to the actual produced power. At AM5 for instance, the solar radiation conveys only half as much power as under AM1.5. The significant decrease of PCE of HCMJSC designs as compared with the other two structures thus leads only to a small power loss [see Fig. 4(b)].

We now look at the result of AM sensitivity on averaged yearly production. Using the PVLib library,[35] we computed the yearly AM distributions for two locations often used in the literature: Solar Village in Saudi Arabia (latitude 24.54, longitude 46.2) and Golden, Colorado, USA (latitude 39.75, longitude −105.21) [Fig. 5(a)]. The profile of both distributions differs significantly, as the sun is on average much closer to zenith in Solar Village than in Golden (the median AMs are 1.66 and 2.10, respectively).

Following a similar analysis as Hirst et al.,[17] we compute the yearly averaged efficiencies, which corresponds to the nominal efficiency multiplied by the performance factor [see Fig. 5(b)]. As expected, all technologies operate at a lower average efficiency than their nominal values. Furthermore, the average efficiency is higher for low latitudes than for high latitudes, because all technologies are less efficient for AMs superior to 1.5. No matter the type of solar spectrum, HCSCs are systematically less impacted by the spectral distribution, as observed by Hirst et al.[17] (although the difference we find between both technologies is much smaller). High-bandgap HCMJSCs are impacted in much the same way as MJSCs, while low-bandgap HCMJSCs are the most sensitive. In addition, low-latitude illumination conditions comparatively favor hot-carrier based technologies that operate best at low air masses. In all cases, the variations remain small, and therefore all technologies can be considered viable for low and high latitudes.

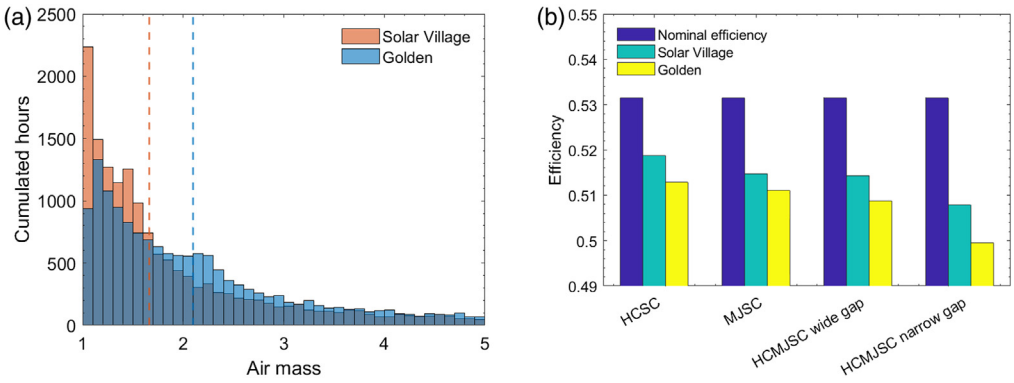

Fig. 5 (a) Cumulative distribution of illumination hours as a function of AM (grouped in steps of 0.1) over one year in two different locations: Solar Village and Golden. The dashed lines indicate the median AM for each location. (b) Averaged efficiency of the four devices shown in Fig. 3 for both locations, compared with their nominal efficiency.

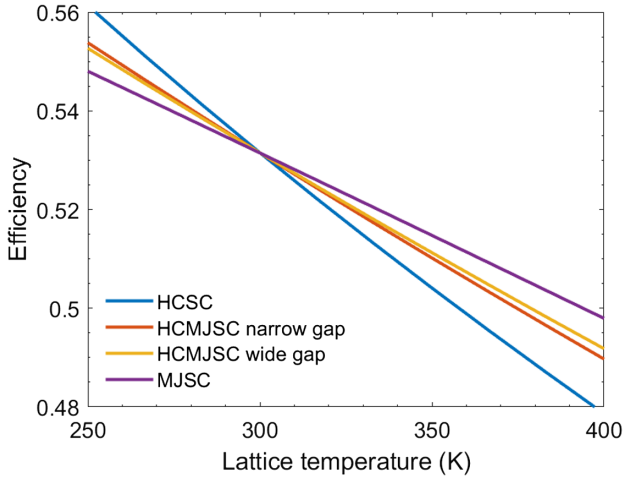

Fig. 6 Efficiency of the four devices shown in Fig. 3 as a function of the lattice temperature. We only consider the explicit dependence on lattice temperature.

4.2 *Nonstandard Temperature*

Finally, we briefly consider the explicit impact of temperature. As a standard, nominal efficiency are estimated at 25°C. Yet, systems in operating conditions reach much higher temperatures, even exceeding 100°C under a 1000 sun illumination.[36] This temperature increase has both direct and indirect impacts of devices' efficiency.[9,10,37] The detailed balance equations have indeed explicit dependence on temperature, notably through the Generalized Planck Law [Eq. (3)] and the thermalized power [Eq. (13)]. In addition, several parameter may vary with temperature, such as bandgap and radiative efficiency. In this preliminary analysis, we only consider explicit temperature dependence of the device presented in Fig. 3 to estimate their fundamental temperature coefficient, as introduced in Ref. 9.

Results are presented in Fig. 6. We find relative degradations of $-0.10\%/\mathrm{K}$ for the HCSC, $-0.080\%/\mathrm{K}$ and $-0.076\%/\mathrm{K}$ for narrow-gap and wide-gap HCMJSCs, respectively, and $-0.063\%/\mathrm{K}$ for MJSCs. These values are of the same order of magnitude as fundamental temperature coefficients reported for single junctions.[9] We note that the HCSC shows (perhaps surprisingly) a stronger temperature dependence than the other concepts. It appears indeed that, while increasing the ambient temperature favors the hot carriers effect in Eq. (13), it reduces the hot-to-ambient temperature ratio, which is detrimental to the cell's voltage [Eq. (11)]. This sensitivity is reduced in the HCMJSC architecture, the behavior of which is closer to that of a standard MJSC.

5 Conclusions

The HCMJSC architecture offers more degrees of freedom when designing the solar cell, making it able to achieve efficiencies comparable to those of HCSCs and MJSCs with fewer constraints. As a result, HCMJSCs are more resilient to nonoptimal design and internal nonidealities. They offer a promising route to take advantage of the hot carrier effect even with materials showing limited thermalization coefficients. However, once these degrees of freedom are optimized for particular illumination conditions, the device is slightly more sensitive to spectral variations than the other two technologies. It is nevertheless possible to design the cell so as to favor resilience, for instance by selecting a larger bandgap for the top absorber. The system's resilience to temperature is more complex to assess, because of the many indirect consequences of a temperature increase. The fundamental temperature coefficient of the HCMJSC lies between that of MJSC and HCSC. A more detailed analysis would be required to conclude on the robustness of these cells in real operation conditions.

Acknowledgments

This study was carried out within the framework of the International Research Network NextPV (CNRS, France and RCAST, the University of Tokyo, Japan), and of the program 6: PROOF (Proof of concept for PV innovation breakthrough) at IPVF (Programme d'Investissement d'Avenir – Grant No. ANR-IEED-002-01). It benefited from the Energy4Climate Interdisciplinary Center (E4C) of IP Paris and École des Ponts ParisTech through the 3rd Programme d'Investissements d'Avenir [ANR-18-EUR-0006-02]. The authors acknowledge fruitful discussions with Jordi Badosa. The authors declare having no conflicts of interest.

Code, Data, and Materials Availability

Numerical results are available upon request to the authors.

References

1. W. Shockley and H. J. Queisser, "Detailed balance limit of efficiency of *p-n* junction solar cells," *J. Appl. Phys.* **32**, 510–519 (1961).
2. J.-F. Guillemoles et al., "Guide for the perplexed to the Shockley-Queisser model for solar cells," *Nat. Photonics* **13**, 501–505 (2019).
3. M. A. Green, *Third Generation Photovoltaics Advanced Solar Energy Conversion*, Springer, Berlin, Heidelberg (2003).
4. R. T. Ross and A. J. Nozik, "Efficiency of hot-carrier solar energy converters," *J. Appl. Phys.* **53**, 3813–3818 (1982).
5. P. Würfel, "Solar energy conversion with hot electrons from impact ionisation," *Sol. Energy Mater. Sol. Cells* **46**, 43–52 (1997).
6. G. Conibeer et al., "Hot carrier solar cells," Chapter 12 in *Advanced Concepts in Photovoltaics*, A. J. Nozik, G. Conibeer, and M. C. Beard, Eds., Energy and Environment Series, pp. 379–424, Royal Society of Chemistry, Cambridge (2014).
7. L. C. Hirst et al., "Hot-carrier solar cell spectral insensitivity: Why develop the hot-carrier solar cell when we have multi-junction devices?" *Proc. SPIE* **8981**, 89810I (2014).
8. A. L. Bris et al., "Thermalisation rate study of GaSb-based heterostructures by continuous wave photoluminescence and their potential as hot carrier solar cell absorbers," *Energy Environ. Sci.* **5**(3), 6225–6232 (2012).
9. O. Dupré, R. Vaillon, and M. Green, "Physics of the temperature coefficients of solar cells," *Sol. Energy Mater. Sol. Cells* **140**, 92–100 (2015).
10. R. Vaillon et al., "Solar cells operating under thermal stress," *Cell Rep. Phys. Sci.* **1**, 100267 (2020).
11. P. Faine et al., "The influence of spectral solar irradiance variations on the performance of selected single-junction and multijunction solar cells," *Sol. Cells* **31**, 259–278 (1991).
12. H. Shpaisman et al., "Can up- and down-conversion and multi-exciton generation improve photovoltaics?" *Sol. Energy Mater. Sol. Cells* **92**, 1541–1546 (2008).
13. M. Yoshida et al., "Photon ratchet intermediate band solar cells," *Appl. Phys. Lett.* **100**, 263902 (2012).
14. A. Delamarre et al., "An electronic ratchet is required in nanostructured intermediate-band solar cells," *IEEE J. Photovoltaics* **8**, 1553–1559 (2018).
15. A. Delamarre et al., "Non-ideal nanostructured intermediate band solar cells with an electronic ratchet," *Proc. SPIE* **10527**, 105270R (2018).
16. S. Philipps et al., "Energy harvesting efficiency of III-V triple-junction concentrator solar cells under realistic spectral conditions," *Sol. Energy Mater. Sol. Cells* **94**, 869–877 (2010).
17. L. Hirst et al., "Spectral sensitivity of hot carrier solar cells," *Sol. Energy Mater. Sol. Cells* **120**, 610–615 (2014).
18. M. Giteau, S. Almosni, and J.-F. Guillemoles, "Hot-carrier multi-junction solar cells: a synergistic approach," *Appl. Phys. Lett.* **120**, 213901 (2022).
19. J. Guillemoles et al., "Guide for the perplexed to the shockley-queisser model for solar cells," *Nat. Photonics* **13**, 501–505 (2019).

20. M. Giteau et al., "Detailed balance calculations for hot-carrier solar cells: coupling high absorptivity with low thermalization through light trapping," *EPJ Photovoltaics* **10**, 1 (2019).
21. P. Wurfel, "The chemical potential of radiation," *J. Phys. C Solid State Phys.* **15**(18), 3967 (1982).
22. D.-T. Nguyen et al., "Quantitative experimental assessment of hot carrier-enhanced solar cells at room temperature," *Nat. Energy* **3**, 236–242 (2018).
23. A. D. Vos, "Detailed balance limit of the efficiency of tandem solar cells," *J. Phys. D Appl. Phys.* **13**, 839–846 (1980).
24. A. L. Bris et al., "Hot carrier solar cells: controlling thermalization in ultrathin devices," *IEEE J. Photovoltaics* **2**, 506–511 (2012).
25. M. Giteau et al., "Identification of surface and volume hot-carrier thermalization mechanisms in ultrathin GaAs layers," *J. Appl. Phys.* **128**, 193102 (2020).
26. A. Le Bris and J.-F. Guillemoles, "Hot carrier solar cells: achievable efficiency accounting for heat losses in the absorber and through contacts," *Appl. Phys. Lett.* **97**, 113506 (2010).
27. A. Le Bris et al., "Hot carrier solar cells: controlling thermalization in ultrathin devices," *IEEE J. Photovoltaics* **2**, 506–511 (2012).
28. Y. Rosenwaks et al., "Hot-carrier cooling in GaAs: quantum wells versus bulk," *Phys. Rev. B* **48**, 14675–14678 (1993).
29. L. C. Hirst et al., "Enhanced hot-carrier effects in InAlAs/InGaAs quantum wells," *IEEE J. Photovoltaics* **4**, 1526–1531 (2014).
30. G. Conibeer et al., "Towards an understanding of hot carrier cooling mechanisms in multiple quantum wells," *Jpn. J. Appl. Phys.* **56**, 091201 (2017).
31. H. Esmaielpour et al., "Exploiting intervalley scattering to harness hot carriers in III–V solar cells," *Nat. Energy* **5**, 336–343 (2020).
32. J. W. M. Lim et al., "Spotlight on hot carriers in halide perovskite luminescence," *ACS Energy Lett.* **7**, 749–756 (2022).
33. A. Bett et al., "III-V compounds for solar cell applications," *Appl. Phys. A* **69**, 119–129 (1999).
34. C. Gueymard, "SMARTS, a simple model of the atmospheric radiative transfer of sunshine: algorithms and performance assessment," Tech. Rep. FSEC-PF-270-95, Florida Solar Energy Center (1995).
35. W. F. Holmgren, C. W. Hansen, and M. A. Mikofski, "pvlib python: a python package for modeling solar energy systems," *J. Open Source Software* **3**, 884 (2018).
36. C. Algora and I. Rey-Stolle, *Handbook of Concentrator Photovoltaic Technology*, John Wiley & Sons Inc., Hoboken (2016).
37. J. J. Wysocki and P. Rappaport, "Effect of temperature on photovoltaic solar energy conversion," *J. Appl. Phys.* **31**, 571–578 (1960).

Maxime Giteau is a postdoctoral researcher at C2N, CNRS, France. He received his MSc degree in engineering and solid state physics, respectively, from Supaero and Paul Sabatier University, France, in 2016, and his PhD from the University of Tokyo, Japan, in 2020. His current research interests include theoretical and practical aspects of light trapping as well as high-efficiency photovoltaic concepts, in particular hot-carrier solar cells.

Samy Almosni is a senior researcher at Saule Technologies. He obtained his MSc degree in nanotechnologies from the University of Versailles, France, in 2011 and his PhD in optoelectronic from Institut des Sciences Appliquées de Rennes, France, in 2015. He is currently working on the development of perovskite solar cells and is interested in high-efficiency concepts.

Jean-François Guillemoles is a CNRS research director, head of the IPVF joint lab (CNRS- E. Polytechnique- ENSCP-and SAS IPVF), Paris-Saclay (France) aiming at the development of photovoltaics, and former director of a joint lab with the University of Tokyo, NextPV. He is currently active on high efficiency concepts for solar energy conversion, new applications for photovoltaic, luminescence-based characterization techniques (esp. hyperspectral imaging), and modeling of photovoltaic materials and devices. He is a part-time professor at École Polytechnique. He is author/coauthor of more than 400 publications (peer-reviewed papers, book

chapters, patents, proceedings, etc.) and editor for *Progress in Photovoltaics* (Wiley) and *EPJ Photovoltaics* (EDP).

Daniel Suchet is a professor at École Polytechnique and a researcher at Institut du Photovoltaïque d'Île de France (IPVF), Palaiseau, France. He received his engineering degree from École Polytechnique in 2014 and prepared his PhD on ultracold atoms at the Laboratoire Kastler Brossel in Paris. He then turned to solar energy at NextPV (University of Tokyo, Japan), and is currently working on advanced concepts for solar energy conversion.